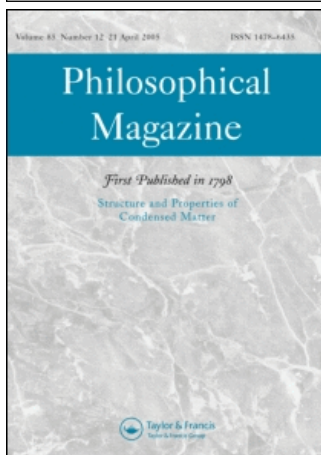


This article was downloaded by:[Ma, X. L.]
On: 30 August 2007
Access Details: [subscription number 781668196]
Publisher: Taylor & Francis
Informa Ltd Registered in England and Wales Registered Number: 1072954
Registered office: Mortimer House, 37-41 Mortimer Street, London W1T 3JH, UK



Philosophical Magazine

First published in 1798

Publication details, including instructions for authors and subscription information:
<http://www.informaworld.com/smpp/title~content=t713695589>

Asymmetrical twin boundaries and highly dense antiphase domains in $\text{BaNb}_{0.3}\text{Ti}_{0.7}\text{O}_3$ thin films

Online Publication Date: 01 October 2007

To cite this Article: Zheng, S. J. and Ma, X. L. (2007) 'Asymmetrical twin boundaries and highly dense antiphase domains in $\text{BaNb}_{0.3}\text{Ti}_{0.7}\text{O}_3$ thin films', Philosophical Magazine, 87:28, 4421 - 4431

To link to this article: DOI: 10.1080/14786430701541138

URL: <http://dx.doi.org/10.1080/14786430701541138>

PLEASE SCROLL DOWN FOR ARTICLE

Full terms and conditions of use: <http://www.informaworld.com/terms-and-conditions-of-access.pdf>

This article maybe used for research, teaching and private study purposes. Any substantial or systematic reproduction, re-distribution, re-selling, loan or sub-licensing, systematic supply or distribution in any form to anyone is expressly forbidden.

The publisher does not give any warranty express or implied or make any representation that the contents will be complete or accurate or up to date. The accuracy of any instructions, formulae and drug doses should be independently verified with primary sources. The publisher shall not be liable for any loss, actions, claims, proceedings, demand or costs or damages whatsoever or howsoever caused arising directly or indirectly in connection with or arising out of the use of this material.

© Taylor and Francis 2007

Asymmetrical twin boundaries and highly dense antiphase domains in $\text{BaNb}_{0.3}\text{Ti}_{0.7}\text{O}_3$ thin films

S. J. ZHENG^{†‡} and X. L. MA^{*†}

[†]Shenyang National Laboratory for Materials Science, Institute of Metal Research,
Chinese Academy of Sciences, 110016 Shenyang, China

[‡]Graduate School of Chinese Academy of Sciences, 100049 Beijing, China

(Received 6 March 2007; accepted in revised form 27 June 2007)

Asymmetrical twin boundaries and highly dense antiphase domains were identified by means of transmission electron microscopy in a perovskite-based $\text{BaNb}_{0.3}\text{Ti}_{0.7}\text{O}_3$ thin film grown by laser molecular beam epitaxy on a SrTiO_3 (001) substrate. The microstructural characteristics of the $\text{BaNb}_{0.3}\text{Ti}_{0.7}\text{O}_3$ film were clarified in terms of lamellar {111} twins and antiphase domains, the domain boundaries of which are $1/2\langle 110 \rangle$ stacking faults. It is proposed that the intersections of (111) twinning with the antiphase domain boundaries result in the asymmetrical twin boundaries.

1. Introduction

Much attention has been paid to perovskite-based oxides due to their promising superconducting, ferroelectric, ferromagnetic and optical properties [1–9]. Ferroelectric BaTiO_3 is one of the most important perovskite oxide materials in electronics owing to its various device applications [3, 4]. An interesting feature of BaTiO_3 is that its electrical properties can be effectively tuned by incorporation of dopants. For example, in pure BaTiO_3 , there is no mobile carrier, which makes it an insulator. When doped with Nb^{5+} , some free electrons are introduced into the film with Nb^{5+} substituted for Ti^{4+} and therefore the doped BaTiO_3 becomes an n-type semiconductor.

Studies of niobium doping on the crystal structure have been extensively performed [10–15], although there are some deviations among different results [10–13]. It is known that the lattice parameters increase with increasing niobium content while the c/a ratio decreases. In the high niobium content range, Guo *et al.* [11] reported that with the further increase of niobium content up to nearly 10%, the c/a ratio of lattice parameters saturates; above 10 at.% Nb doping, the BaTiO_3 thin films are transformed into a disordering cubic structure.

*Corresponding author. Email: xлма@imr.ac.cn

A study on electrical resistivity shows that Nb-doped BaTiO₃ thin films display a similar value to that of a Nb-doped BaTiO₃ single crystal [10]. Recently, Yan *et al.* [14] studied in detail the electrical properties of Nb-doped BaTiO₃ thin films on a SrTiO₃ substrate with niobium content ranging from 1% to 30%. With increasing Nb content, there is a proportional increase in the carrier density, but the resistivity only reduces by a factor of about three. On the other hand, for a fixed value of 30%, when the oxygen pressure increases during deposition, the resistivity of the Nb-doped BaTiO₃ thin films increases, but the n-type carrier concentration decreases. Guo *et al.* [15] have also systematically investigated the Nb-doped BaTiO₃ thin films with niobium content ranging from 1% to 50% on an MgO substrate. Hall measurements at room temperature show that with the increasing niobium content, the resistivity of Nb-doped BaTiO₃ thin films decreases, whereas the carrier concentration and carrier mobility increase. Moreover, the optical transmittance reduces with an increase of the niobium contents.

Although much work has been carried out on Nb-doped BaTiO₃ films, little has yet been done on the detailed microstructural characterization of such films, especially on the defect configuration within the films. In the present study, we report detailed microstructural characteristics in a BaNb_{0.3}Ti_{0.7}O₃ (BNT0) thin film grown on a SrTiO₃ (STO) substrate. The present study is expected to provide some information useful to the understanding of physical properties and to feed back some data for the better control of the film growth.

2. Experimental procedures

A BaNb_{0.3}Ti_{0.7}O₃ thin film with a thickness of 300 nm was grown by laser molecular beam epitaxy (LMBE). The base pressure of the epitaxy chamber was 1×10^{-8} Pa. The output of a Lambda Physik LEXTRA 200 excimer laser (308 nm, 20 ns, 2 Hz) was used as the laser source with energy density of about 1 J cm^{-2} . A piece of single-crystal SrTiO₃ (STO) and a piece of sintered BNT0 (with an Nb doping content of 30 at.%) were used as the targets. Before deposition, the STO (001) substrate was annealed at 660°C for 20–30 min in an oxygen atmosphere (1×10^{-4} Pa) to clear the surface. Subsequently, 20 unit cells of STO were homoepitaxially grown on the substrate to reduce the defect density and to smooth the surface. Then the BNT0 thin film was grown with a deposition rate of about 0.01 nm/pulse, and the distance between the target and substrate was 60 mm. The deposition temperature was 610°C and the oxygen pressure was 6.0×10^{-1} Pa. During deposition of both STO and BNT0 films, the observed fine streaky reflection high-energy electron diffraction (RHEED) patterns and undamping HREED intensity oscillations indicate that the films were two-dimensionally epitaxially grown on STO (001) substrate.

The cross-section and plan-view specimens for TEM observation were prepared by the conventional processes of slicing, grinding and final ion-milling. A Tecnai G² F30 transmission electron microscope was used for electron diffraction and atomic imaging.

3. Experimental results and discussion

3.1. Cross-sectional and plan-view observations

Figure 1 shows a low-magnification cross-section TEM image and its corresponding selected-area electron diffraction (SAED) pattern with incident electron beam parallel to the $[100]$ direction of the STO substrate. The interface between the BNTO film and the STO substrate is flat and sharp. It can be seen that a significant amount of columnar structures, revealed by dark contrast bands, originate from the interface and extend vertically to the surface of the BNTO film. The SAED pattern shown in figure 1b is a composite of two sub-patterns from the film and the substrate. Since the lattice parameter of the BNTO film is larger than that of the STO substrate, the spots split circumferentially to the transmission spot. In addition, the diffraction spots parallel to the BNTO/STO interface are elongated, implying that some highly dense planar defects exist, the boundaries of which are perpendicular to the interface. The diffraction spot splitting and their elongation are clearly seen in the rectangular frame labelled A and their enlargement.

When we tilted the specimen about the $[001]$ axis of STO from $[100]$ to $[1\bar{1}0]$, we found a number of lamellae with darker contrast in the film, the width of which ranges from 10 to 30 nm, as shown in figure 2a. Such lamellae lay along $+28^\circ$ and -28° ($90^\circ - \alpha$ in figure 2a) apart from the interface normal and they originate near the interface and run through the film. Figure 2b shows the composite SAED pattern corresponding to the area in figure 2a with incident electron beam parallel to the $[1\bar{1}0]$ direction of the STO substrate. The splitting of

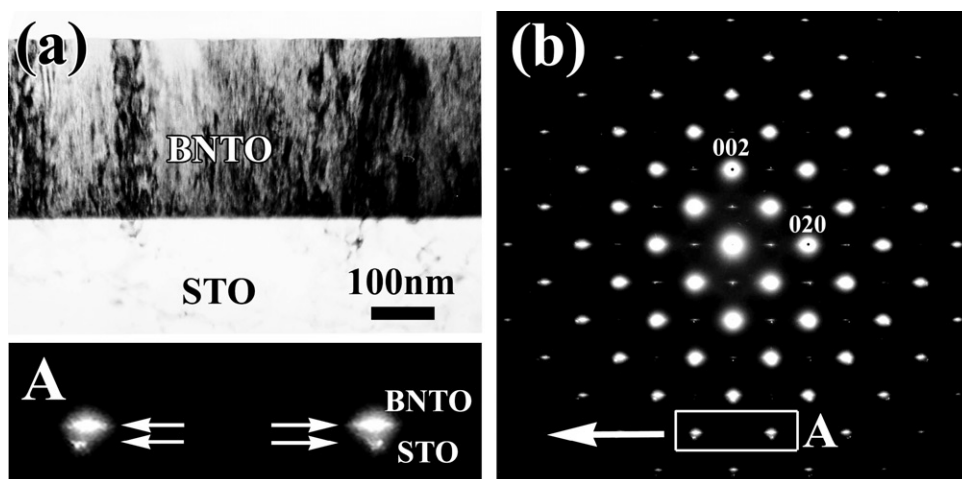


Figure 1. (a) A low-magnification cross-section TEM image and (b) corresponding SAED pattern with incident electron beam parallel to the $[100]$ direction of STO substrate. It is seen that a great deal of columnar structures featured by dark contrast bands originate from the interface and extend vertically to the surface of BNTO film. The SAED pattern is a composite of two sub-patterns from the film and the substrate.

diffraction spots due to difference of film/substrate lattice parameters and the elongation of diffractions owing to planar defects (to be discussed later) in the film can be clearly seen, particularly in the enlarged white rectangular frame labelled A. In such SAED patterns, $(\bar{1}\bar{1}1)$ and (111) twins are also identified. The $(\bar{1}\bar{1}1)$ twin relations are indicated by solid and broken rectangles with their origin at the incident beam of the electron diffraction patterns (EDPs). Some of the spots marked with arrows in the EDPs result from secondary diffraction. The BNTO matrix diffraction spots, the indexes of which are labelled with subscript m, are connected by a solid line frame and the twin diffraction spots are connected by a broken line frame. It should be mentioned that, for a cubic or pseudo-cubic structure when viewed along the $[1\bar{1}0]$ direction, the (111) plane should be 35.3° apart from the interface normal. However, in the present film, as shown in figure 2a, the angle is determined to be 28° . Hence, the twins do not exactly lie on $\{111\}$ planes, resulting in asymmetrical twin boundaries. Such asymmetrical twin boundaries result from the interaction of the (111) twin and the antiphase domain boundaries to be discussed in section 3.3.

Figure 3a shows a low-magnification plan-view TEM image of the film showing the lamellar $\{111\}$ twins when the twin boundaries are edge-on under near the $[01\bar{1}]$ direction. Figure 3b shows the EDP corresponding to the TEM image in figure 3a. It is a composite EDP involving twinning on two $\{111\}$ planes. Figures 3c and 3d show dark-field micrographs imaged with diffractions from variant twin lamellae, which clearly show the distribution of each group of twinning.

3.2. Structures of antiphase domains

In addition to the asymmetrical twin boundaries, another salient feature in the BNTO film is the formation of highly dense antiphase domains. Figure 4 shows a

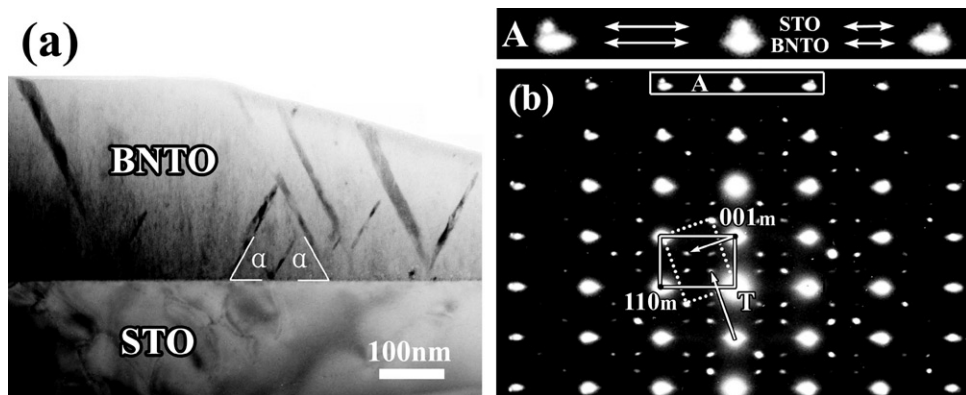


Figure 2. (a) A low-magnification cross-section TEM image of BNTO/STO and (b) the corresponding SAED pattern taken along the $[1\bar{1}0]$ direction. In (a), a number of lamellae is shown, the width of which ranges from 10 nm to 30 nm, with darker contrast in the film. Such lamellae lay along $+28^\circ$ and -28° ($90^\circ - \alpha$) apart from the interface normal and they originate near the interface and run through the film.

low-magnification plan-view image showing the distribution of the antiphase domain boundaries in the film. An HRTEM image showing the details of the domain boundaries is shown in figure 5. It is found that antiphase domain boundaries mainly lie on $\{100\}$ and $\{110\}$ planes. Domain B is shifted by $1/4[110]$ and $1/4[1\bar{1}0]$ with respect to domain A, which is indicated by the white circuit in figure 5. According to Lu *et al.* [16], such antiphase domain boundaries are edge-on $1/2 \langle 110 \rangle$ stacking faults. In order to understand the three-dimensional structure of antiphase domains, the $[1\bar{1}0]$ and $[100]$ directions are imaged using the cross-section specimen.

Figure 6a shows the $[1\bar{1}0]$ HRTEM image, on which three antiphase domains are labelled A, B and C. The relative shift between domains in the $[001]$ direction

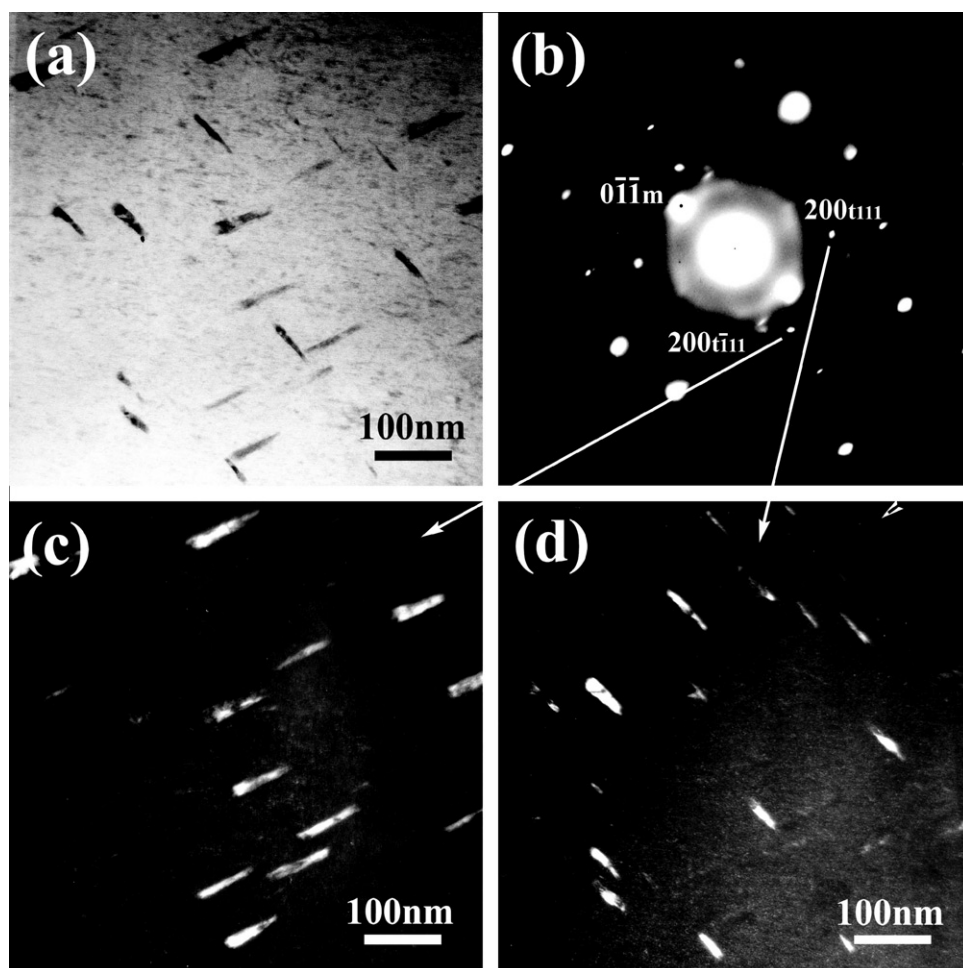


Figure 3. (a) A low-magnification plan-view TEM image of the film showing the lamellar $\{111\}$ twins when the twin boundaries are edge-on in the viewing direction close to $[01\bar{1}]$. (b) Composite EDPs corresponding to (a). (c, d) Dark-field micrographs imaged with diffractions from variant twin lamellae.

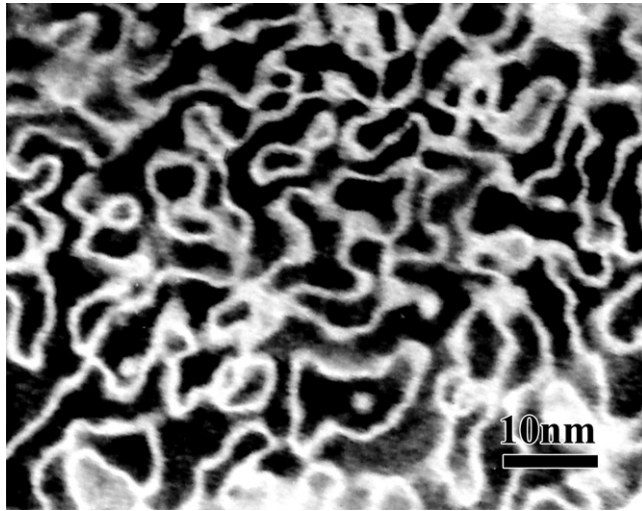


Figure 4. A low-magnification plan-view image showing the distribution of the antiphase domain boundaries in the film.



Figure 5. An HRTEM image showing the antiphase domain boundary structure. It can be seen that antiphase domain boundaries mainly lie on $\{100\}$ and $\{110\}$ planes. The white circuit is a rectangle, and the bottom left vertex of the rectangle does not lie on a bright image spot of domain B, whereas the other three vertices lie on bright image spots of domain A. Hence, it shows the relative shift between domain A and B.

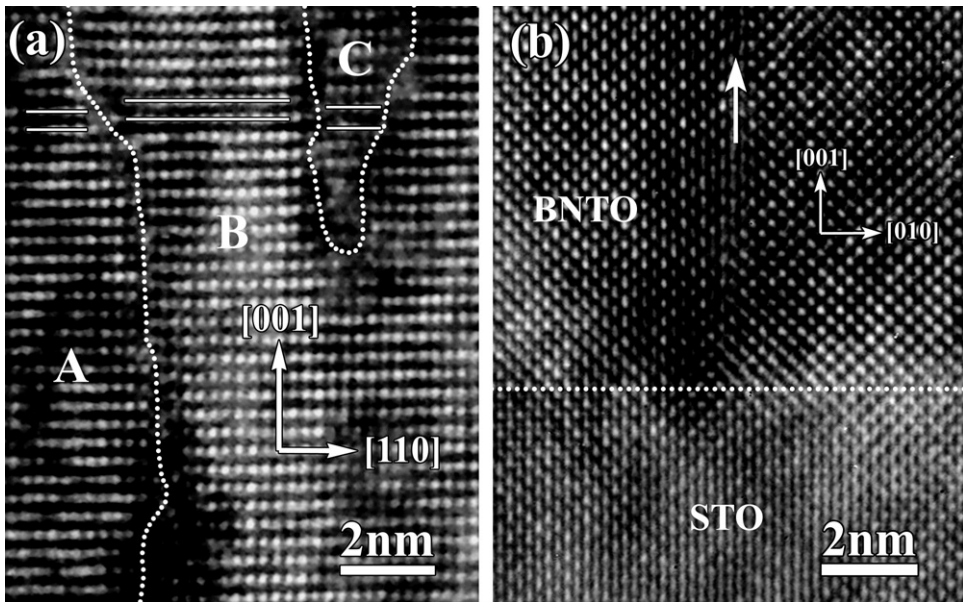


Figure 6. HRTEM images showing the antiphase domain boundary structure in (a) $[1\bar{1}0]$ and (b) $[100]$ directions. Except for domain C in (a), most of the antiphase domains originate from the BNTO/STO interface and extend vertically to the surface of the film.

is indicated by horizontal lines. It is noticeable that the antiphase domain boundaries, which are labelled by dashed lines, are meandering. It is found that most of these domains originate at the interface between the film and the substrate. Figure 6b shows the $[100]$ HRTEM image, where again we can find that the antiphase domain boundary, indicated by a white arrow, forms at the interface and extends vertically to the surface of the BNTO film. These antiphase domains correspond to the columnar structures observed in figure 1a. It is the high density of such domains that results in the elongation of diffraction spots parallel to the interface, as shown in figure 2b.

3.3. Intersection of the $\{111\}$ twin and the antiphase domain

Figure 7 shows an HRTEM image of a lamellar $(\bar{1}\bar{1}1)$ twin taken along the $[1\bar{1}0]$ zone axis of the matrix. It is of interest to note that the twin boundary is composed of a number of sections, and each of these sections, connected by steps (marked with arrows), is a $(\bar{1}\bar{1}1)$ twin. The combination of these sections results in the overall boundary apart from the $(\bar{1}\bar{1}1)$ plane of the film, forming an asymmetrical twin boundary. The formation of these asymmetrical twin boundaries actually results from the interaction of the $(\bar{1}\bar{1}1)$ twin and the antiphase domains.

Figure 8 is an enlargement of the region labelled A in figure 7, showing the details of the interaction. It can be seen that a step results from an interaction between the twin boundary and antiphase domain boundaries denoted with dashed lines. It is

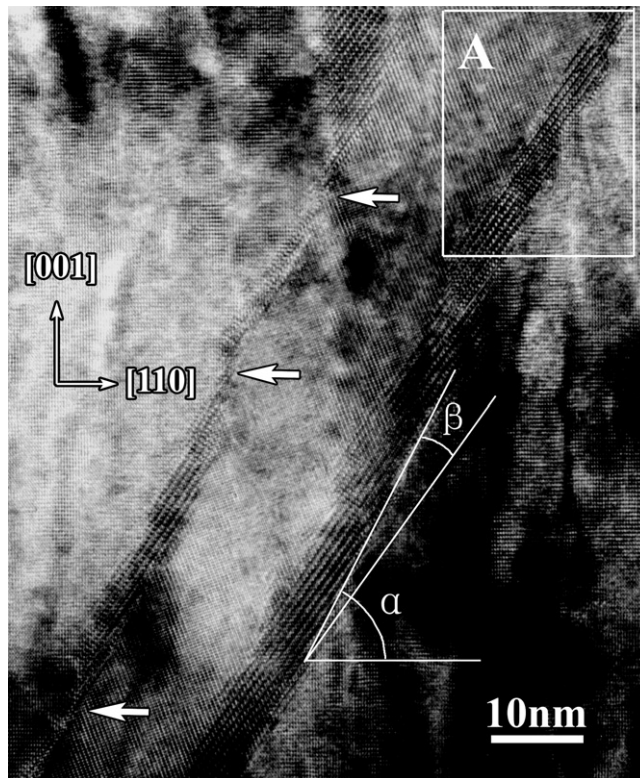


Figure 7. An HRTEM image of a lamellar $(\bar{1}\bar{1}1)$ twin taken along $[1\bar{1}0]$ zone axis of matrix. It is of interest to note that the twin boundary is composed of a number of sections, and each of these sections, connected by steps, is $(\bar{1}\bar{1}1)$ twin. Steps are marked with arrows, and between them are sections of the boundary. The combination of these sections results in the overall boundary apart from the $(\bar{1}\bar{1}1)$ plane of the film, forming an asymmetrical twin boundary. The angle of the boundary apart from the $(\bar{1}\bar{1}1)$ plane, which is marked with β , is about 8° , while the definition of α is the same as mentioned above. The formation of these asymmetrical twin boundaries actually results from the interaction of $(\bar{1}\bar{1}1)$ twin and antiphase domains.

proposed that the epitaxial film grows along the $[001]$ direction layer by layer, as do the antiphase domains, the boundaries of which lie on (100) , (010) , (110) and $(\bar{1}10)$. However, the lamellar $(\bar{1}\bar{1}1)$ twin grows along the $[112]$ direction. Antiphase domains might make the twin boundary rise vertically, thereby forming steps along the boundary.

Figure 9 schematically illustrates the interaction between twins and antiphase domains. Region A is linked with C by twinning, but with B by an antiphase domain boundary. The two boundaries are labelled using a solid line and a dashed line, respectively. It can be seen that the interaction between the twin boundary and the antiphase domain boundary make the twin boundary rise vertically, thereby form the step indicated by b-c.

In addition, it should be mentioned that the asymmetrical twin boundaries are not edge-on along $\langle 110 \rangle$ zone axes, since in the joint area of the two counterparts



Figure 8. An enlargement of the region labelled by A in figure 7, which shows the details of the interaction of (111) twin and antiphase domains. Domain boundaries are indicated by dashed lines. Steps appear at the interaction areas pointed out by arrows.

of the twins we observe a lattice spacing three times that of the (111) spacing. Such a large lattice spacing results from the overlap of the two counterparts of the twins.

4. Conclusions

By means of transmission electron microscopy, microstructures in a $\text{BaNb}_{0.3}\text{Ti}_{0.7}\text{O}_3$ thin film were clarified in terms of lamellar {111} twinning and antiphase domains. The boundaries of the antiphase domains are determined to be $1/2\langle 110 \rangle$ stacking faults. It is also found that these stacking faults intersect with twin boundaries, which result in asymmetrical twin boundaries. The asymmetrical twin boundaries in the present study are not edge-on along the $\langle 110 \rangle$ direction, since in the joint area of the two counterparts of the twins we can see a lattice spacing of three times that of the (111) spacing, which results from the overlap of the two counterparts of the twins along the viewing direction.

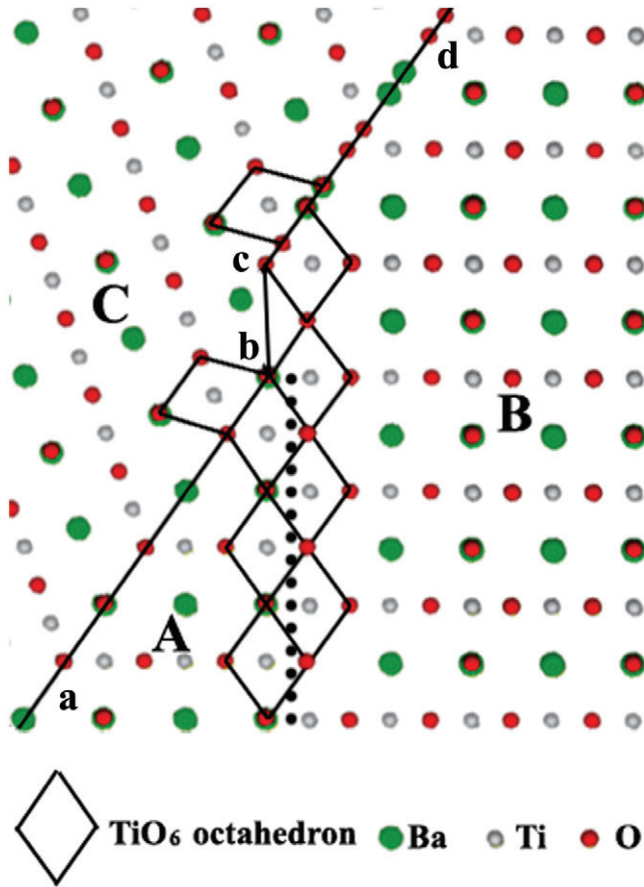


Figure 9. Schematic illustration showing the interaction between the (111) twin and an antiphase domain. The twin boundary is labelled a-b and c-d. Region A is linked with C by twinning, but with B by the antiphase domain boundary. The boundaries are labelled with solid and dashed lines, respectively.

Acknowledgments

We would like to thank Professor H. B. Lu, Institute of Physics, Chinese Academy of Sciences, for providing the samples. This work was supported by the National Natural Science Foundation of China with Grant No. 50325101 and Special Funds for the Major State Basic Research Projects of China (Grant No. 2002CB613503).

References

- [1] J.G. Bednorz and K.A. Muller, *Z. Phys. B* **64** 198 (1986).
- [2] C.W. Chu, H.P. Hor, R.L. Meng, *et al.*, *Science* **235** 567 (1987).

- [3] M. Sayer and K. Screenivas, *Science* **247** 1056 (1990).
- [4] R.E. Cohen, *Nature* **358** 136 (1992).
- [5] R. Von Helmolt, J. Wecker, B. Holzapfel, *et al.*, *Phys. Rev. Lett.* **71** 2331 (1993).
- [6] S. Jin, T.H. Tiefel, M. McCormack, *et al.*, *Science* **264** 413 (1994).
- [7] A. Urushibara, Y. Moritomo, T. Arima, *et al.*, *Phys. Rev* **51** 14103 (1995).
- [8] K. Chahara, T. Ohno, M. Masahiro, *et al.*, *Appl. Phys. Lett.* **63** 1990 (1993).
- [9] C. Kwon, M.C. Robson, K.C. Kim, *et al.*, *J. Magn. Magn. Mater.* **172** 229 (1997).
- [10] D. Nagano, H. Funakubo, K. Shinozaki, *et al.*, *Appl. Phys. Lett.* **72** 2017 (1998).
- [11] H.Z. Guo, L.F. Liu, S. Ding, *et al.*, *J. Appl. Phys.* **96** 3404 (2004).
- [12] L.F. Liu, H.Z. Guo, H.B. Lu, *et al.*, *J. Appl. Phys.* **97** 054102 (2005).
- [13] Y.S. Kim, C.H. Chen, A. Saiki, *et al.*, *J. Phys.* **D 35** 1499 (2002).
- [14] L. Yan, H.B. Lu, Z.H. Chen, *et al.*, *J. Cryst. Growth* **244** 225 (2002).
- [15] H.Z. Guo, L.F. Liu, H.B. Lu, *et al.*, *Chin. Phys. Lett.* **21** 396 (2004).
- [16] C.J. Lu, L.A. Bendersky, K. Chang, *et al.*, *Phil. Mag.* **83** 1565 (2003).